MECHANICAL BEHAVIOUR OF HYBRID 3D WOVEN COMPOSITES UNDER STATIC AND IMPACT LOADINGS

Raúl Muñoz[a], Francisca Martínez[a], Rocío Seltzer[a], Carlos González[a,b,*], Javier Llorca[a,b]

[a]*IMDEA Materials Institute, C/Eric Kandel, 2, 28906 Getafe, Madrid, Spain*
[b]*Polythecnic University of Madrid, Department of Material Science, E. T. S. de Ingenieros de Caminos, Ciudad Universitaria, 28040 Madrid*
**carlosdaniel.gonzalez@imdea.org*

Keywords: 3D woven, hybrid composites, impact, damage

Abstract
This work presents a comprehensive experimental characterisation of a hybrid 3D composite material subjected to in-plane tensile and low-velocity impact loadings. The specimens were manufactured using hybrid 3D orthogonal preforms made of three fibre types: S2-glass, T700 carbon and UHMWPE Dyneema. The laminate lay-up was asymmetric, having a high concentration of CF on one side and GF on the other. A detailed inspection of post-mortem specimens was conducted by means of X-ray computer tomography to ascertain the deformation and damage mechanisms. Results show that hybridisation and 3D weaving can be used to improve the energy absorption capability and the ductility of polymer-matrix composites.

1. Introduction

Standard composite materials are manufactured by stacking plies containing either unidirectional or bidirectional fiber tows or fabrics. This approach is ideal to maximize the in-plane composite properties as the fibers, which provide stiffness and strength, are oriented within the plane. However, the out-of-plane properties of these 2D laminates are limited. This is particularly critical under out-of-plane impact because interply decohesion may develop even in the absence of visible damage in the top and bottom plies [1]. These delaminations lead to major reductions in the compressive strength because the laminate is subdivided into thinner sublaminates with lower buckling load. One successful strategy to improve the out-of-plane mechanical properties of the 2D laminates has been the development of 3D fabrics by binding 2D preforms in the out-of-plane direction using either z-pinning, stitching or weaving. In particular, woven orthogonal preforms have gained rapid impulse, since traditional 2D weaving machines could be adapted to build these 3D fabrics. Furthermore, the resulting composites made by polymer infusion of the 3D fabrics (hereafter called 3D composites) have shown outstanding mechanical properties in terms of damage tolerance [2,3], delamination resistance, notch sensitivity [2], and energy absorption during out-of-plane impact [4] as compared with the 2D counterparts [5]. This work presents the experimental results from tensile in-plane [6] and out-of-plane low velocity impact [7] tests for a new kind of 3D composite materials obtained by the in-plane hybridisation of glass and carbon tows, and weaving across the thickness with Dyneema binders.

2. Materials and experimental techniques

The 3D composite was supplied by 3Tex. A non-crimp 3D orthogonal preform (Figure 1a). was vacuum infused with Derakane 8084. The laminate was made up by alternating layers formed by fiber tows oriented in the warp and weft directions. In this case, the hybrid composite had 2.5 consecutive warp and weft layers made from carbon fiber, followed by 4.5 consecutive warp and weft layers made from S2 glass fiber, Fig. 1b. The z-yarn binder was made up of ultra-high molecular weight polyethylene (PE) fiber (Dyneema). It should be noticed that the lay-up of the hybrid 3D composite was not symmetric.

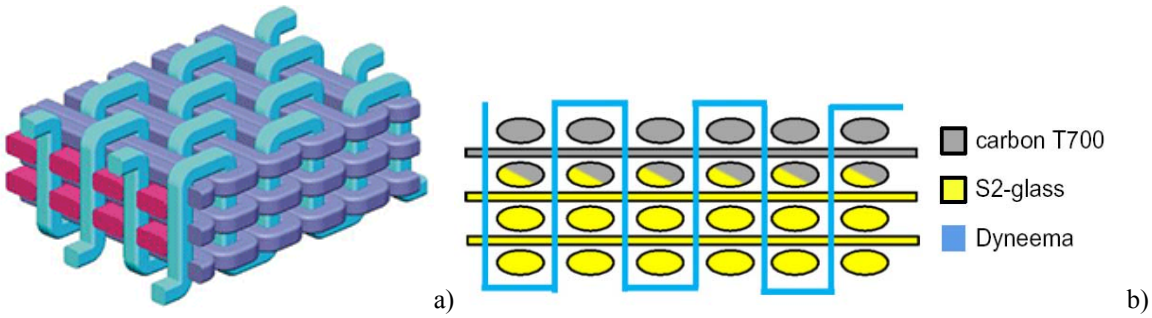

Figure 1. a) Non-crimp 3D Orthogonal fiber architecture from www.3tex.com, b) detail of the hybrid configuration.

Rectangular specimens of 250x25x4.1 mm^3 were machined from the plate with the longest dimension aligned in either the warp or the fill direction for the tensile tests. Glass fiber tabs of 50 mm in length were glued to the specimens, leading to a free length of 150 mm. They were tested in tension in an electromechanical universal testing machine (Instron 3384) following the recommendations of the ASTM D3039. Tests were carried out under stroke control at 2 mm/min and the load was continuously measured during the test with a load cell of 150 kN. Since composite is non-symmetric (and coupling between bending and extension might occur), the longitudinal strain was recorded on both faces of the specimen using an extensometer of 50 mm gage length on one face and digital image correlation (Vic2D) on the other. Periodic unloading-reloading was carried out in one test in each direction (warp or fill) to estimate the stiffness degradation as a function of the applied strain.

Low-velocity impact tests were carried out using an Instron Dynatup 8250 drop weight testing machine. Square specimens of 145x145 mm^2 were cut from the composite panels. The composite plates were simply supported by the fixture and held at the corners with special clamping tweezers, leading to a free impact area of 127x127 mm^2. The specimens were impacted at the center using a 12.7 mm diameter steel tup. Incident impact energies in the range 21–316 J were chosen by selecting the weight and the initial position of the impactor to obtain at least two tests with full penetration and another two tests without full penetration. The height of the tup was adjusted to obtain an impact velocity of ≈4 m/s in all cases to avoid strain rate effects and differences in the noise amplitude, which are proportional to the impact velocity [20]. The impactor was instrumented with a 50 kN load cell and an accelerometer to record continuously the applied force P, the tup displacement d, and the velocity v.

X-ray Computer Tomography XCT of the specimens was performed with a Nanotom 160NF (Phoenix) at 70-90 kV and 120-180 mA using a W target. 1800 radiographs were acquired for each tomogram with an exposure time of 1000ms. The reconstructed volumes presented a resolution of 13-15 μm/voxel. Emphasis was placed on the qualitative assessment of the main

damage mechanism in each material as a function of applied strain rather than in the quantification of specific damage modes (delaminated surface, volume of cracked tows, fraction of broken fibers, etc.). The damage micromechanisms in the composite specimens after testing were analysed as a function of the load by means of XCT. Specimen were immersed in dye penetrant liquid to enhance the visualization of the cracks. The liquid was composed of 60 g of ZnI in 10 ml of water, 10 ml of ethanol and 10 ml of Kodak Photo-Flo 200.

3. Tensile behaviour

Three tensile tests were carried out in the fill and warp directions. The corresponding stress-strain curves are plotted in Figs. 2a and 2b. The strains were measured by conventional extensometry on the glass face of the coupon and by digital image correlation on the carbon face. The differences in the strain between both faces were negligible, indicating that the extension-bending coupling induced by the asymmetry of the composite did not play a significant role in the tensile behavior at least until the fracture of the carbon fibers. The stress-strain curves in the fill direction (Fig. 2a) presented a linear-elastic behavior up to a strain in the range 1.2% to 1.6%, which is similar to the failure strain of the carbon fiber tows. There was a sudden drop in the load bearing capacity of the composite but the load increased slightly with further strain until catastrophic failure, which occurred at an applied strain below 2.5%.

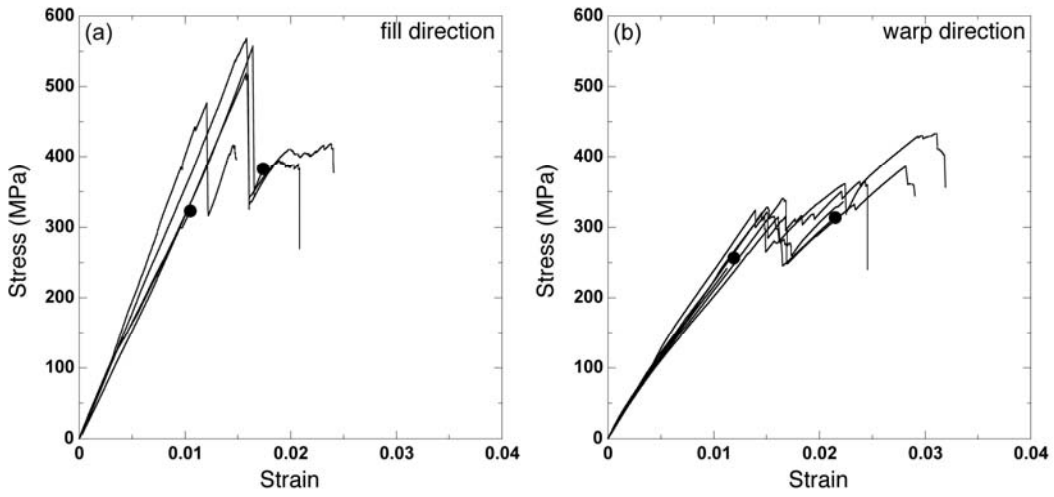

Figure 2. Stress-strain curves of the plain composite coupons. (a) Fill direction. (b) Warp direction. The solid circles in the curves indicate the instants in which the test was stopped and the coupons were examined by means of XCT.

The initial part of the stress-strain curve was also linear in the warp direction (Fig. 2b), but a slight non-linearity was detected before the load peak, which occurred when the applied strain was in the range 1.3% to 1.7%, as in the fill direction. Nevertheless, the load bearing capacity of the composite increased with further straining and the maximum strength was attained for applied strains in the range 2.1% to 3.1%, just before the coupon failed catastrophically. This failure strain is compatible with the development of damage in the glass fiber tows. Thus, composite coupons loaded in tension along the fill and warp direction presented two peaks. The maximum strength along the fill direction was attained in the first peak and it was controlled by the fracture of the AS4C carbon fiber yarns. The maximum strength in the warp direction was attained in the second peak and it was controlled by the fracture of the S2 glass

fiber tows. It should be noted that the main differences in the composite architecture between the fill and warp direction were the presence of an extra hybrid ply with the fibers oriented in the fill direction and that the PE z-yarn binders were oriented along the warp direction.

3.1 Damage mechanisms

XCT was carried out in one coupon deformed in the fill direction and deformed up to strains of 1.05% and 1.74% (marked with solid circles in Fig. 3a). The first analysis occurred in the linear region of the stress-strain curve, before carbon fiber breakage took place. Two cross-sections of the investigated volume parallel to the loading axis are shown in Figs. 3a and 3b. Bright regions in the tomograms correspond to cracks (or pores), whose contrast was enhanced by the presence of ZnI. The two sections in Fig. 3 are parallel and one of them (Fig. 3b) contains the PE z-yarns, which run in the vertical direction. The two carbon layers running in the fill and warp directions are at the top in Fig. 3, and the missing yarn every other yarn in the warp direction is clearly visible in Fig. 3a. The four glass fiber layers are at the bottom and the hybrid layer (light grey/dark grey contrast) is in between. The resin- rich area due to the missing yarn enhanced crimping of the adjacent carbon and carbon/glass yarns in the fill directions, leading to delamination of the fill tows from the matrix (marked with arrows).

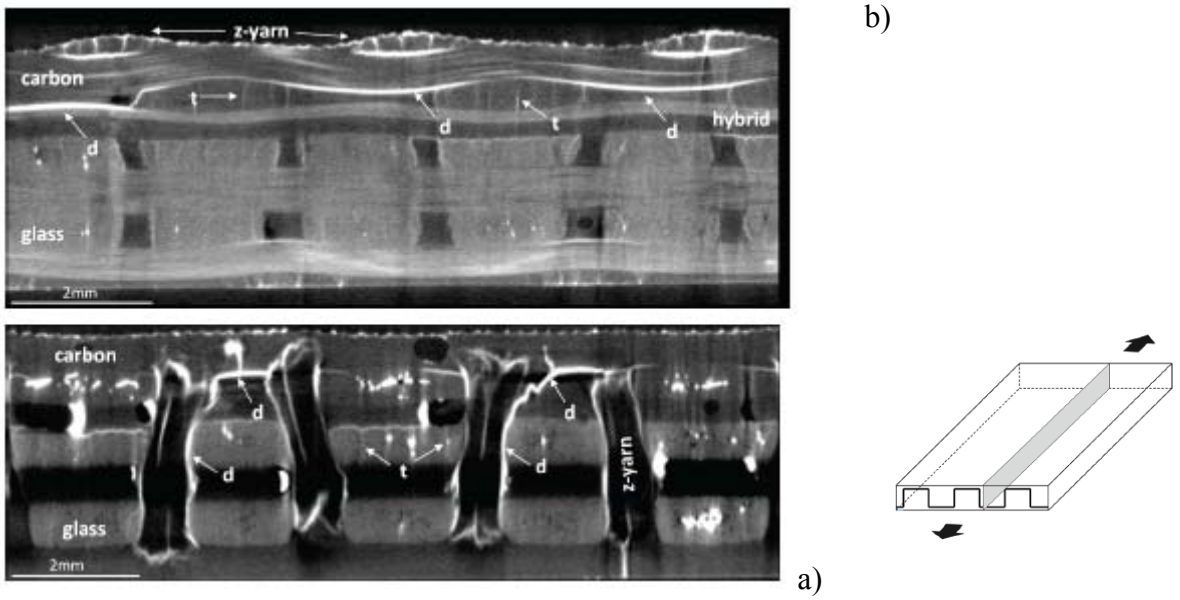

Figure 3. Tomograms of the coupon loaded in the fill direction up to 1.05% strain (a) Longitudinal section parallel to the (horizontal) loading axis (b) Another longitudinal section parallel to the (horizontal) loading axis which contains the PE z-yarns.

These delamination cracks propagated along the tows. Note that delamination was asymmetric: only the upper or the lower tow boundary was delaminated from the matrix. In addition, tensile transverse cracks were observed in the fiber tows oriented in the warp direction (perpendicular to the tensile loading). These cracks propagated through the matrix (and along the interface) within the fiber tows. The parallel cross-section in Fig 3b depicted the same failure mechanisms (namely, delamination of the carbon and hybrid fill tows from the matrix near the missing warp tows and tensile cracking of the warp tows) but it is worth noting that the PE z-yarns arrested the propagation of the delamination cracks. In addition, delamination of PE z-yarns was also evident (marked with arrows).

XCT was also carried out in one coupon deformed in the warp direction at strains of 1.19% and 2.15% (marked with solid circles in Fig. 2b). The tomograms of cross-sections parallel and perpendicular to the loading axis deformed up to 1.19% are depicted in Figs. 4a and 4b, respectively. The main damage mechanisms observed in the longitudinal sections which did not contain PE z-yarns were fiber tow delamination and tensile transverse cracks within the fiber tows (Fig. 4a). Delamination cracks were occasionally detected into the fiber tows, propagated across the tow and led to another delamination crack at the opposite tow surface. The sections containing PE z-yarns also showed extensive delamination of the PE yarns from the matrix and carbon and glass fiber tows, while delamination cracks between matrix and carbon or glass were arrested by the z-yarns (Fig. 4b).

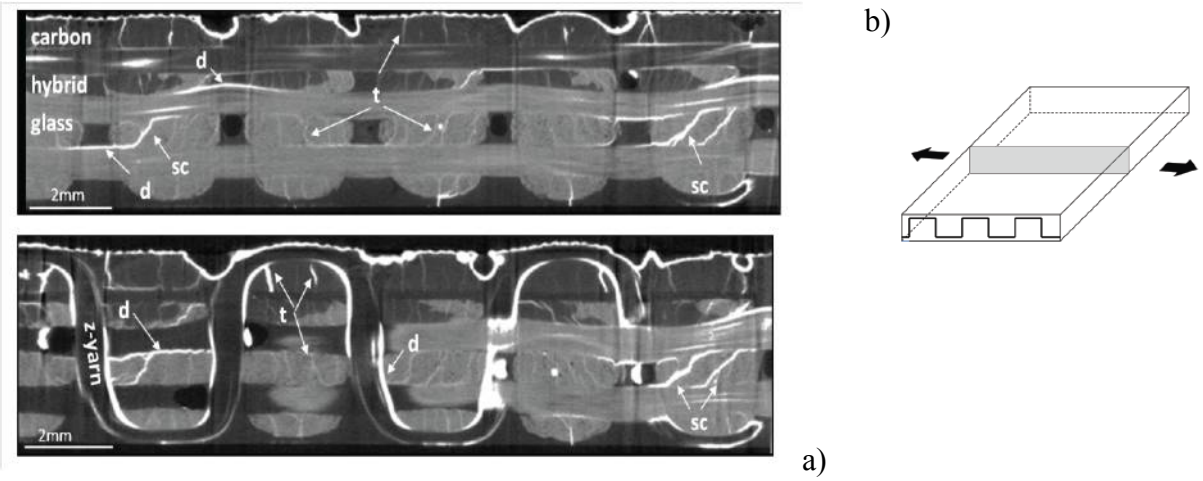

Figure 4. Tomograms of the coupon loaded in the warp direction up to 1.19% strain. (a) Longitudinal section parallel to the (horizontal) loading axis (b) Another longitudinal section parallel to the (horizontal) loading axis which contains the PE z-yarns.

4. Low-velocity impact

A minimum of four impact tests were carried out on each material. Impact energies were selected so that full penetration was achieved in at least two specimens. Load was alternatively applied on the carbon and the glass sides to evaluate the influence of hybridisation. Representative load–displacement (P–d) and energy displacement (U-d) curves corresponding to impact energies of 94J and 164J are plotted in Figs. 5a–d. They stand for one test in which full penetration was achieved and another test in which the tup was stopped before reaching the maximum load. The different P–d curves presented consistent results and the scatter was very limited. The mechanical response was initially smooth and the impact energy was spent in the elastic deformation of the plate as well as in damage.

The analysis of the hibridisation revealed that when the load was applied on the glass fiber face, (Hybrid_GF label in Figure 5), the material underwent larger plastic deformation and fracture than in the carbon face (Hybrid_CF). High frequency oscillations in the load were observed in all P–d curves prior to the maximum load. They were caused by the brittle fracture of the fibers in tension in the backside surface of the plate as a result of bending. The absorbed energies were calculated as the area below the load-displacement curves, as shown in Figures 5a and b. The initial stiffness was the same in both plate configurations, while the peak load was higher for the Hybrid_CF plate. From the impacts without penetration it is noted that Hybrid_CF stored ≈30 % of the impact energy as elastic potential, whereas the

Hybrid_GF transforms most of it into plastic deformation and fracture. Furthermore, upon penetration, Hybrid_CF presented the largest ability to absorb energy.

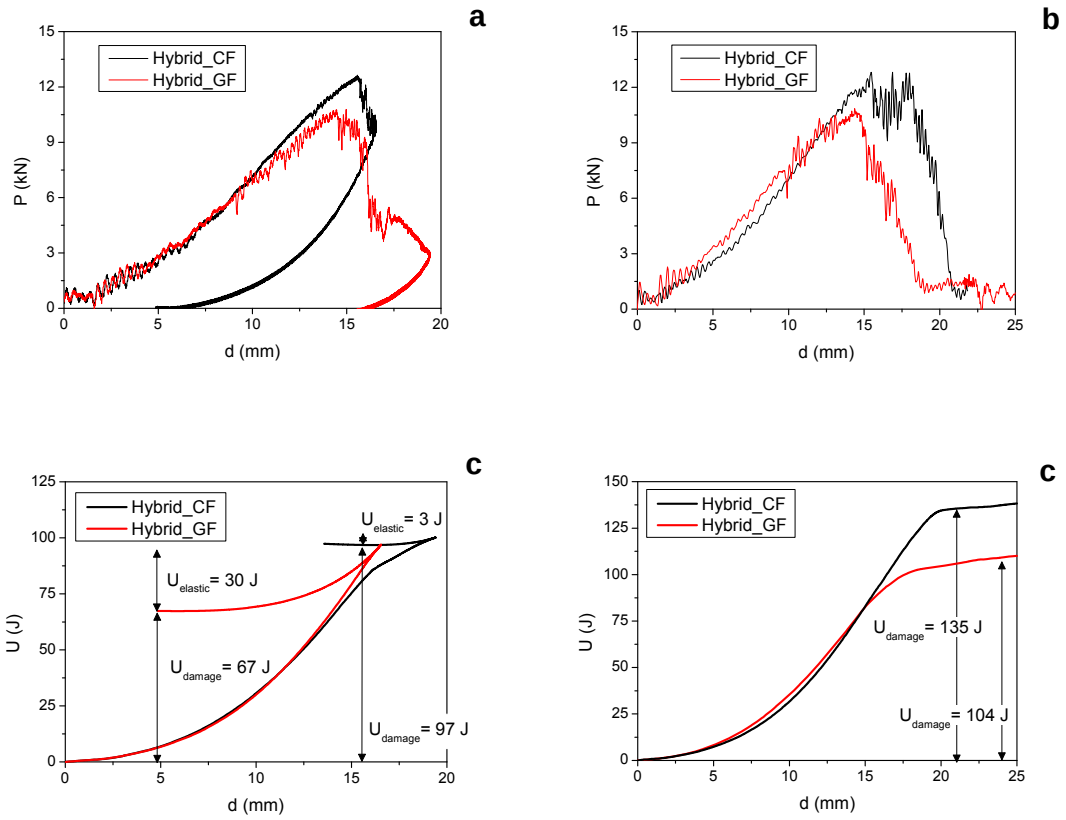

Figure 5. Load – displacement (P-d) and energy – displacement (U-d) records of the hybrid plates impacted with an energy of (a, c) 94 J and (b, d) 162 J.

4.1 Damage mechanisms

Results from XCT inspection of impacted specimens are depicted in Figure 6. GF appears in yellow, while CF, Dyneema and the epoxy-vinylester matrix appear in grey. These last three components have similar colour due to the fact that they have similar X-ray absorption coefficients.

Although specimens impacted at higher energies resulted in larger damage area, most of the damage mechanisms were common to penetrated and non-penetrated specimens. As shown in Figure 6, evidence of intratow matrix cracking micromechanisms was found, including matrix cracking and fragmentation due to tensile stresses at the bottom of the plates –where the largest in-plane tensile stresses occur–; matrix crushing close to the impacted region due to out-of-plane compressive stresses; shear fracture due to out-of-plane shear stress and tow splitting due to in-plane shear stresses. Moreover, z-yarn debonding due to poor adhesion of polyethylene (Dyneema) with epoxy vinylester, matrix cracking in resin pockets located at the tows cross-over sites and fiber brooming (i.e. transversal fracture of fibers at different lengths) at the rear layer –where tensile stresses predominate– were also detected.

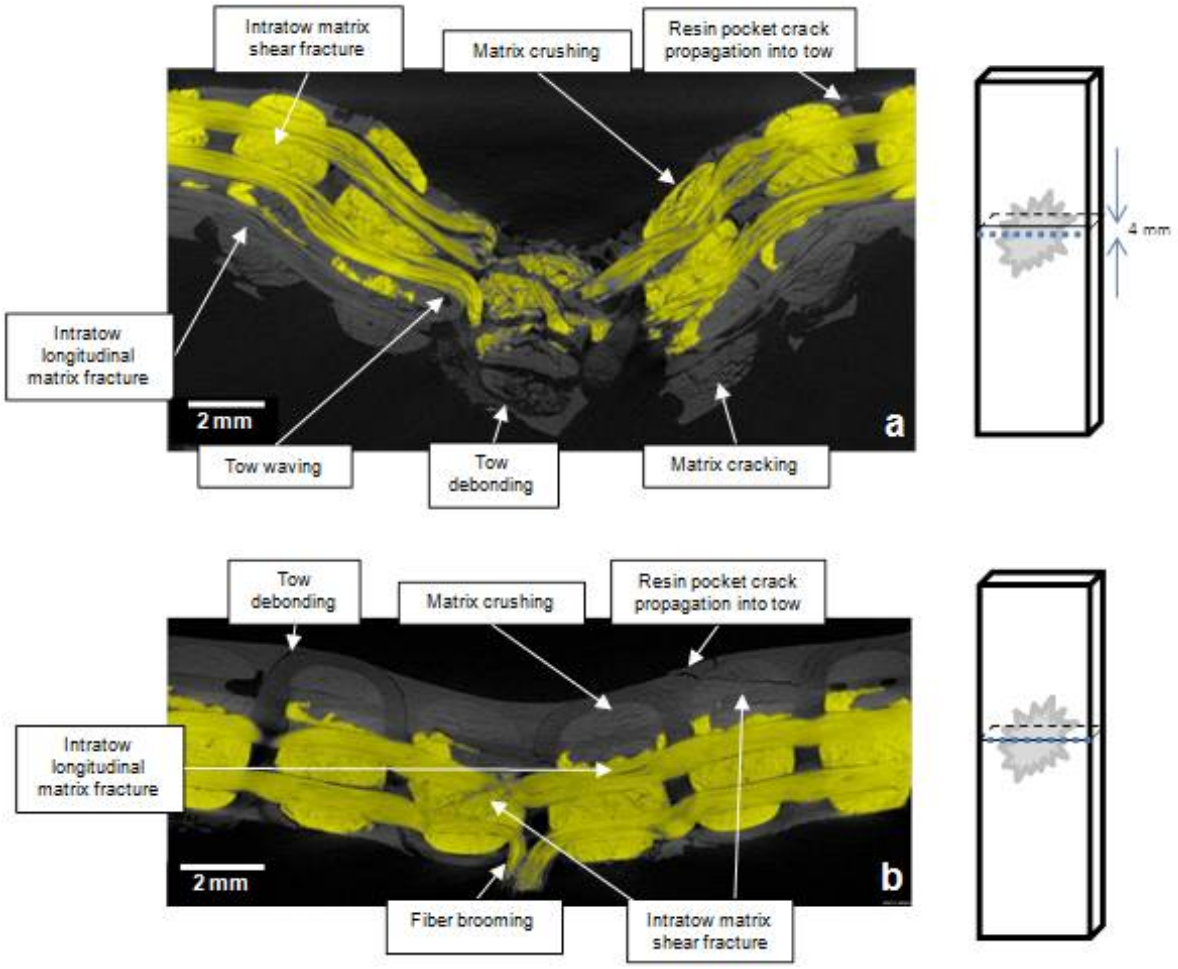

Figure 6. XCT cross-sections of the imprints left on (a) Hybrid_GF and (b) Hybrid_CF after an impact of 94 J. The schemes at the right show their locations. GF are coloured in yellow, while CF, Dyneema and resin are in grey.

5. Conclusions

The in-plane tensile and impact response of a hybrid 3D woven composite showed to be highly dependent on the test configuration. In the case of the tensile tests, the strength was controlled by the ductility of the individual yarns, being the strength larger in the fill direction due to the higher volume fraction of carbon fibers (composite failure strain of ≈1.5%). Contrary, when straining in the warp direction, glass fiber yarns led to a more ductile behaviour reaching failure strains up to ≈3%. XCT revealed extensive tow cracking and z-yarn debonding promoting the progressive damage in the composite laminate, but finally, the strength was controlled totally by the volume fraction of yarns in each direction. In the case of the low-velocity impact tests, the absorbed energy increased in ≈30% when the plate was impacted on the CF rich side, rather than on the GF rich side. Tomographic imaging demonstrated that in the former case the rigid CF layers under compression delayed the GF layers deformation and subsequent failure, resulting in a more resilient and tougher configuration.

References

[1] Schoeppner GA, Abrate S. Delamination threshold loads for low velocity impact on composite laminates. Composites: Part A 2000;31:903–15.

[2] Cox BN, Dadkhah MS, Morris WL, Flintoff JG. Failure mechanisms of 3D woven composites in tension, compression, and bending. Acta Metall Mater 1994; 42(12):3967–84.

[3] Cox BN, Dadkhah MS, Morris WL. On the tensile failure of 3D woven composites. Compos Part A: Appl Sci Manuf 1996;27(6):447–58.

[4] Ko FK, Hartman D. Impact behavior of 2-D and 3-D glass/epoxy composites. SAMPE J 1986;22(4):26–30.

[5] Enfedaque A, Molina-Aldareguía JM, Gálvez F, González C, Llorca J. Effect of glass fiber hybridization on the behavior under impact of woven carbon fiber/ epoxy laminates. J Compos Mater 2010;44(25):3051–68.

[6] R. Muñoz, V. Martínez, F. Sket, C. González, J. LLorca, Mechanical behavior and failure micromechanisms of hybrid 3D woven composites in tension, Composites Part A: Applied Science and Manufacturing, 59, 2014, 93–104

[7] R. Seltzer, C. González, R. Muñoz, J. LLorca, T. Blanco Varela, X-ray microtomography analysis of the damage micromechanisms in 3D woven composites under low-velocity impact, Composites: Part A 45 (2013) 49–60